EurJIC
European Journal of Inorganic Chemistry

Research Article
doi.org/10.1002/ejic.202200416

Chemistry Europe
European Chemical Societies Publishing

www.eurjic.org

Cationic Nickel d^9-Metalloradicals [Ni(NHC)$_2$]$^+$

Lukas Tendera,[a] Martin S. Luff,[a] Ivo Krummenacher,[a] and Udo Radius*[a]

A series of five new homoleptic, linear nickel d^9-complexes of the type [Ni^I(NHC)$_2$]$^+$ is reported. Starting from the literature known Ni(0) complexes [Ni(Mes$_2$Im)$_2$] **1**, [Ni(Mes$_2$Im^{H2})$_2$] **2**, [Ni(Dipp$_2$Im)$_2$] **3**, [Ni(Dipp$_2$Im^{H2})$_2$] **4** and [Ni(cAAC^{Me})$_2$] **5** (Mes$_2$Im = 1,3-bis(2,4,6-trimethylphenyl)-imidazolin-2-ylidene, Mes$_2$Im^{H2} = 1,3-bis(2,4,6-trimethylphenyl)-imidazolidin-2-ylidene, Dipp$_2$Im = 1,3-bis(2,6-diisopropylphenyl)-imidazolin-2-ylidene, Dipp$_2$Im^{H2} = 1,3-bis(2,6-diisopropylphenyl)-imidazolidin-2-ylidene, cAAC^{Me} = 1-(2,6-diisopropylphenyl)-3,3,5,5-tetramethylpyrrolidin-2-yliden), their oxidized Ni(I) analogues [Ni^I(Mes$_2$Im)$_2$][BPh$_4$] **1**$^+$, [Ni^I(Mes$_2$Im^{H2})$_2$][BPh$_4$] **2**$^+$, [Ni^I(Dipp$_2$Im)$_2$][BPh$_4$] **3**$^+$, [Ni^I(Dipp$_2$Im^{H2})$_2$][BPh$_4$] **4**$^+$ and [Ni^I(cAAC^{Me})$_2$][BPh$_4$] **5**$^+$ were synthesized by one-electron oxidation with ferrocenium tetraphenylborate. The complexes **1**$^+$–**5**$^+$ were fully characterized including X-ray structure analysis. The complex cations reveal linear geometries in the solid state and NMR spectra with extremely broad, paramagnetically shifted resonances. DFT calculations predicted an orbitally degenerate ground state leading to large magnetic anisotropy, which was verified by EPR measurements in solution and on solid samples. The magnetic anisotropy of the complexes is highly dependent from the steric protection of the metal atom, which results in a noticeable decrease of the *g*-tensor anisotropy for the *N*-Mes substituted complexes **1**$^+$ and **2**$^+$ in solution due to the formation of T-shaped THF adducts.

Introduction

Stable two-coordinate, open-shell transition metal complexes have attracted much attention in the last decades[1] due to their high reactivity and very interesting chemical and physical properties, which allow different applications in small molecule activation, catalysis[2] and magnetism.[3] Bulky ligands are usually necessary to stabilize the monomeric complexes,[4] as they tend to decompose, disproportionate, aggregate to oligomers or form larger ionic lattices. Even with such a steric protection of the metal center, these complexes are often very air and moisture sensitive.

In the past years we reported on the use of [Ni^0(NHC)$_2$] synthons in organometallic chemistry and catalysis in stoichiometric[5] and catalytic[6] reactions. We recently highlighted stereo-electronic effects on the reactivity of different *N*-substituted and backbone methylated NHC ligands in the chemistry of [Ni^0(NHC)$_2$] with small molecules such as alkenes, alkynes, carbonyls and aldehydes.[5j,k] This work already revealed that mononuclear, linear nickel complexes [Ni^0(NHC)$_2$] such as [Ni(Mes$_2$Im)$_2$] **1** (Mes$_2$Im = 1,3-bis(2,4,6-trimethylphenyl)-imidazolin-2-ylidene) much more readily transfer electrons to substrates compared to synthons with smaller NHC ligands. Our work on C–F bond activation and defluoroborylation of polyfluoroarenes using the NHC ligated Ni(0) complexes [Ni$_2$(^{i}Pr$_2$Im)$_4$(μ–(η^2:η^2)-COD)][7] and [Ni(Mes$_2$Im)$_2$] **1**[8] revealed that [Ni$_2$(^{i}Pr$_2$Im)$_4$(μ-(η^2:η^2)-COD)] (^{i}Pr$_2$Im = 1,3-diisopropylimidazolin-2-ylidene) favors a concerted (in conjunction with an NHC-assisted) reaction pathway, whereas **1** favors a radical (in conjunction with an NHC-assisted) pathway for the C–F bond activation step.[9] Most interestingly, a detailed exploration of the redox potentials of [Ni(Mes$_2$Im)$_2$] **1** and polyfluorinated arenes revealed that in these cases the radical formation is not due to simple electron transfer from **1** to the fluoroarene but due to the approach of the fluoroarene to the nickel center of **1** and the abstraction of a fluoride atom in the first step of the C–F bond activation process. Similarly, for the borylation of aryl chlorides using **1** as a catalyst[6g] we also excluded one electron transfer from **1** to chloroarenes. However, these studies revealed that the reversible redox potential for the process [Ni(Mes$_2$Im)$_2$] (**1**)→[Ni(Mes$_2$Im)$_2$]$^+$ (**1**$^+$) + e$^-$ lies fairly low, at approximately −1.90 V in THF as a solvent.[8b] Furthermore, we were able to synthesize and characterize (including X-ray diffraction, XRD) the cationic linear complex [Ni^I(Mes$_2$Im)$_2$][BF$_4$] **1**$^{+BF4}$ independently.[9]

As we noticed before that this type of one electron transfer should be very important to many catalytic reactions using nickel complexes [Ni^0(NHC)$_2$] which are ligated with the "classical" five-membered ring Arduengo-carbenes, we initiated a detailed investigation on the redox potentials of these compounds as well as synthesis and characterization of cationic mononuclear Ni(I) complexes [Ni^I(NHC)$_2$]$^+$. In addition to the use in catalysis it has turned out that similar linear coordinated Ni(I) complexes show some interesting properties (see below). Although the examples mentioned below are limited to linear complexes, the nickel(I) oxidation state has been stabilized by many other ligands and in different coordination spheres in the past few years.[1c,10]

[a] L. Tendera, M. S. Luff, Dr. I. Krummenacher, Prof. Dr. U. Radius
Institut für Anorganische Chemie,
Julius-Maximilians-Universität Würzburg,
Am Hubland, 97074 Würzburg, Germany
E-mail: martin.luff@uni-wuerzburg.de
u.radius@uni-wuerzburg.de
http://www.ak-radius.de

Supporting information for this article is available on the WWW under https://doi.org/10.1002/ejic.202200416

Part of the "NHC-Ligands in Organometallic Chemistry and Catalysis" Special Collection.

Research Article
doi.org/10.1002/ejic.202200416

The first neutral NHC-stabilized, two-coordinate Ni(I) complexes were reported in 2008 by Hillhouse and co-workers,[10a] which reacted Sigman's dimer $[(Dipp_2Im)Ni(\mu\text{-}Cl)]_2$[11] ($Dipp_2Im$ = 1,3-bis(2,6-diisopropylphenyl)-imidazolin-2-ylidene) with $NaN(SiMe_3)_2$ or LiN(H)Dipp to yield the heteroleptic Ni(I) complexes $[(Dipp_2Im)Ni\{N(SiMe_3\}_2]$ **A** (see Figure 1) and $[(Dipp_2Im)Ni\{N(H)Dipp\}]$.[11] A few years later this group also reported alkyl- and aryl-substituted derivatives $[(Dipp_2Im)Ni\{CH(SiMe_3\}_2]$ and $[(Dipp_2Im)Ni(dmp)]$ (dmp = 2,6-dimesitylphenyl).[12] The groups of Tilley *et al.*[13] and Power *et al.*[14] independently demonstrated that one-electron reduction of $[Ni^{II}\{N(SiMe_3)Dipp\}_2]$ is suitable to generate anionic, homoleptic complexes of the type $[Cat][Ni^{I}\{N(SiMe_3)Dipp\}_2]$ **B** (cation Cat = K, NBu_4), which were subsequently transformed into neutral Ni(I) complexes by protonation with NEt_3HCl in the presence of neutral two-electron donor ligands, yielding complexes $[(L)Ni^{I}\{N(SiMe_3)Dipp\}]$ (L = $Dipp_2Im$, P^tBu_3, P^iPr_3).[15] In a further ligand exchange reaction the second amido ligand was replaced with dtbmp (dtbmp = 2,6-di-*tert*-butyl-4-methylphenol), which either coordinates *via* the oxygen atom or as an η^5-coordinated phenol ligand, respectively. In 2013, Whittlesey *et al.* reported the linear homoleptic $[Ni^{I}(6\text{-}Mes)_2]^+$ cation **C1** using the six-membered ring *N*-heterocyclic carbene 6-Mes (= 1,3-bis(2,4,6-trimethylphenyl)-3,4,5,6-tetrahydropyrimidin-2-ylidene), which was the first d^9 Ni(I) complex associated with single ion magnet (SIM) behavior. The high magnetic anisotropy of this complex is caused by a very unique orbital splitting resulting in an unquenched angular orbit momentum.[16] Krossing *et al.* reported the related phosphine complex $[Ni^{I}(P^tBu_3)_2]^+$ **D**, which was just the second example for a homoleptic, cationic two-coordinate Ni(I) complex.[17] They also described some structural and magnetic similarities to complex **C1**, but did not identify SIM behavior for this complex. Just recently, Whittlesey and co-workers expanded their work on linear Ni(I) complexes ligated with six- or seven-membered NHC ligands and presented three related complexes $[Ni^{I}(7\text{-}Mes)_2]^+$ **C2**, $[Ni^{I}(6\text{-}Xyl)_2]^+$ **C3**, $[Ni^{I}(7\text{-}Xyl)_2]^+$ **C4** including a detailed discussion about their magnetic properties, focusing on the extreme *g*-tensor anisotropy and its dependence on structural distortion.[18] It was demonstrated that these complexes reveal an orbitally degenerate ground state $^2\Delta$, which results from a unique crystal-field splitting (*vide infra*), and therefore leads to very large magnetic anisotropy. The noticeable differences in the low-temperature magnetic relaxation of these compounds were attributed to different vibrational modes and to spin-phonon coupling, while the different torsion angles of the ligands seem to have no influence on the relaxation times, respectively.[18]

Results and Discussion

We started our investigations with the preparation of a series of five literature known linear Ni(0) complexes ligated with different saturated and unsaturated five-ring NHC ligands or a cyclic (alkyl)(amino)carbene (cAAC) ligand, respectively. The complexes $[Ni(Mes_2Im)_2]$ **1**,[19] $[Ni(Mes_2Im^{H2})_2]$ **2**,[20] $[Ni(Dipp_2Im)_2]$ **3**,[21] $[Ni(Dipp_2Im^{H2})_2]$ **4**[21a] and $[Ni(cAAC^{Me})_2]$ **5**[22] (Mes_2Im^{H2} = 1,3-bis(2,4,6-trimethylphenyl)-imidazolidin-2-ylidene, $Dipp_2Im^{H2}$ = 1,3-bis(2,6-diisopropylphenyl)-imidazolidin-2-ylidene, $cAAC^{Me}$ = 1-(2,6-diisopropylphenyl)-3,3,5,5-tetramethylpyrrolidin-2-yliden) were synthesized by slightly modified published procedures (see Experimental Section). While **1** and **2** were synthesized by a simple ligand exchange reaction starting from $[Ni(\eta^4\text{-}COD)_2]$ and two equivalents of the corresponding NHC, complexes **3**, **4** and **5** were synthesized in two steps *via* a reductive route starting

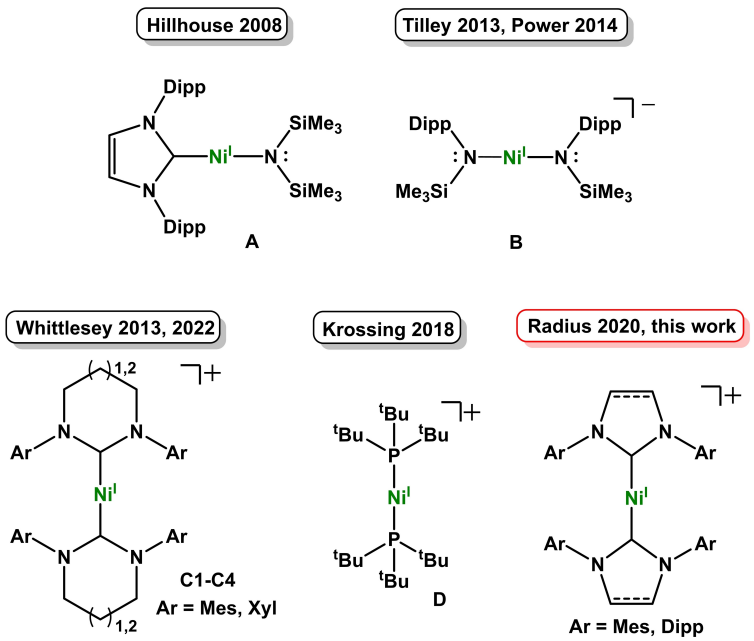

Figure 1. Selected examples of two-coordinated, linear Ni(I) complexes.

Research Article
doi.org/10.1002/ejic.202200416

from $[NiBr_2 \cdot DME]$ and two equivalents of NHC. All compounds **1**–**5** were isolated as black solids which have a dark purple color in solution, and the NMR spectroscopy of these complexes matched the data reported previously.[19–22] As an X-ray structure of complex **2** has not been reported yet, crystals of this compound suitable for XRD were grown from a saturated hexane solution of the complex at −30 °C (Figure 2).

Complex **2** crystallizes in the monoclinic space group $P2_1/c$ and reveals a linear geometry with a $C_{carbene}$–Ni–$C_{carbene}$ angle of 176.46(8)° and Ni–$C_{carbene}$ distances of 1.8187(17) and 1.8332(16) Å, which is perfectly in line with the structural parameters of other complexes $[Ni^0(NHC)_2]$ **1** and **3**–**5** (compare Table 1). The torsion angle between the two planes spanned by the NHC rings (plane N1–C1–N2 – plane N3–C2–N4) of 66.6° is slightly larger than those observed for the other complexes (46.1–60.7°), presumably due to the increasing steric demand of the NHC imposed by the saturated NHC backbone.[19–22]

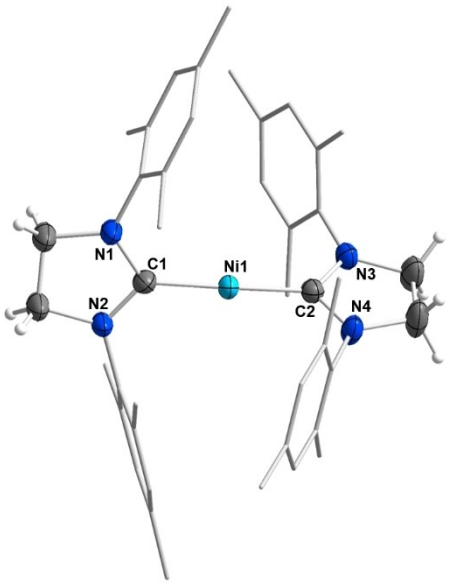

Figure 2. Molecular structure of $[Ni(Mes_2Im^{H2})_2]$ **2** in the solid state (ellipsoids set at the 50% probability level). The hydrogen atoms have been omitted for clarity. Selected bond lengths [Å] and angles [°] of **2**: Ni1–C1 1.8187(17), Ni1–C2 1.8332(16), C1–N1 1.363(2), C1–N2 1.361(2), C2–N3 1.351(2), C2–N4 1.353(2); C1–Ni1–C2 176.46(8), N1–C1–N2 105.99(15), N3–C2–N4 106.64(14), plane (N1–C1–N2) – plane (N3–C2–N4) 66.58(11).

The electronic situation for neutral Ni (d^{10}) complexes $[Ni(NHC)_2]$[23] and cationic Ni (d^9) complexes can be exemplified for the known complexes $[Ni(Mes_2Im)_2]$ **1** and $[Ni(Mes_2Im)_2]^+$ $\mathbf{1}^+$. Density functional theory (DFT) calculations on **1** and $\mathbf{1}^+$ revealed that the energy minimum of both structures optimizes in a D_{2d}-symmetric geometry with distances Ni – $C_{carbene}$ of 1.8457 Å in **1** and 1.9283 Å in $\mathbf{1}^+$, i.e. the Ni–C distances elongate upon oxidation. The electronic structure of the closed-shell species **1** exhibits five occupied metal-based orbitals in an approximate 1:2:2 splitting pattern (Figure 3). The HOMO corresponds to the orbital $32a_1$, which is dominated by Ni d_z2 and s character (an s-d_z2 hybrid orbital, z is the Ni–C axis), and lies at comparable high energies (-3.14 eV). The near-degenerate orbitals $31b_2$ and $15b_2$, which differ by only 0.01 eV in energy, are Ni centered d_{xy} and $d_{x^2-y^2}$ orbitals, and these lie ca. 0.35 eV below the σ-type orbital $32a_1$. These orbitals should be perfectly degenerate e_g orbitals within *pseudo*-$D_\infty h$. Below that lie at −3.78 eV the degenerate orbitals 43e (also e_g in *pseudo*-$D_\infty h$ symmetry), which are d_{xz} and d_{yz} orbitals in character. While a similar 1:2:2 orbital splitting was reported for Pd-$(NHC)_2$,[24] the neutral Ni(0) complex $[Ni(6\text{-}Mes)_2]$ was computed to show a different 2:1:2 splitting where the HOMO corresponds to the d_{xz} and d_{yz} orbitals, followed by the d_z^2 orbital and a low lying set of degenerate d_{xy} and $d_{x^2-y^2}$ orbitals.[16]

However, for the generation of the complex cation $[Ni(Mes_2Im)_2]^+$ $\mathbf{1}^+$, oxidation occurs from the $2e_g$ set of orbitals. The DFT-calculated minimum structure is also of D_{2d} symmetry and oxidation leads to an orbitally degenerated system. The electronic structure of such degenerated systems is not readily

Table 1. Important structural data and magnetic moments in solution (Evans method) of the literature known Ni(0) complexes $[Ni(Mes_2Im)_2]$ **1**,[19] $[Ni(Mes_2Im^{H2})_2]$ **2**,[20] $[Ni(Dipp_2Im)_2]$ **3**,[21] $[Ni(Dipp_2Im^{H2})_2]$ **4**[21a] and $[Ni(cAAC^{Me})_2]$ **5**[22] and their oxidized Ni(I) analogues $[Ni^I(Mes_2Im)_2][BPh_4]$ $\mathbf{1}^+$, $[Ni^I(Mes_2Im^{H2})_2][BPh_4]$ $\mathbf{2}^+$, $[Ni^I(Dipp_2Im)_2][BPh_4]$ $\mathbf{3}^+$, $[Ni^I(Dipp_2Im^{H2})_2][BPh_4]$ $\mathbf{4}^+$ and $[Ni^I(cAAC^{Me})_2][BPh_4]$ $\mathbf{5}^+$.

Compound	Ni–$C_{carbene}$ [Å]	$C_{carbene}$–Ni–$C_{carbene}$ [°]	N–$C_{carbene}$–N/C [°]	Torsion angle [°]	μ_{eff} [μ_B]
1	1.827(6)/ 1.830(6)	176.4(3)	101.5(5)/ 102.5(5)	53.0	–
$\mathbf{1}^+$	1.8954(12)/ 1.8975(13)	179.31(6)	104.19(11)/ 104.27(11)	39.4	2.42
2	1.8187(17)/ 1.8332(16)	176.46(8)	105.99(15)/ 106.64(14)	66.6	–
$\mathbf{2}^+$	1.897(7)/ 1.902(7)	179.8(4)	108.1(6)/ 108.6(6)	32.2	2.49
3	1.856(2)/ 1.872(2)	177.78(10)	101.1(2)/ 101.29(19)	46.1	–
$\mathbf{3}^+$	1.9237(18)/ 1.9312(16)	178.27(7)	103.24(14)/ 103.25(15)	47.4	3.15
4	1.865(3)/ 1.886(3)	177.35(15)	104.1(3)/ 104.3(3)	47.9	–
$\mathbf{4}^+$	1.9734(17)/ 1.9779(16)	179.13(7)	106.91(14)/ 107.15(14)	53.1	2.26
5	1.8419(13)/ 1.8448(14)	166.42(5)	106.40(10)/ 106.49(10)	60.7	–
$\mathbf{5}^+$	1.9311(11)	180	108.29(9)	0	2.82

Research Article
doi.org/10.1002/ejic.202200416

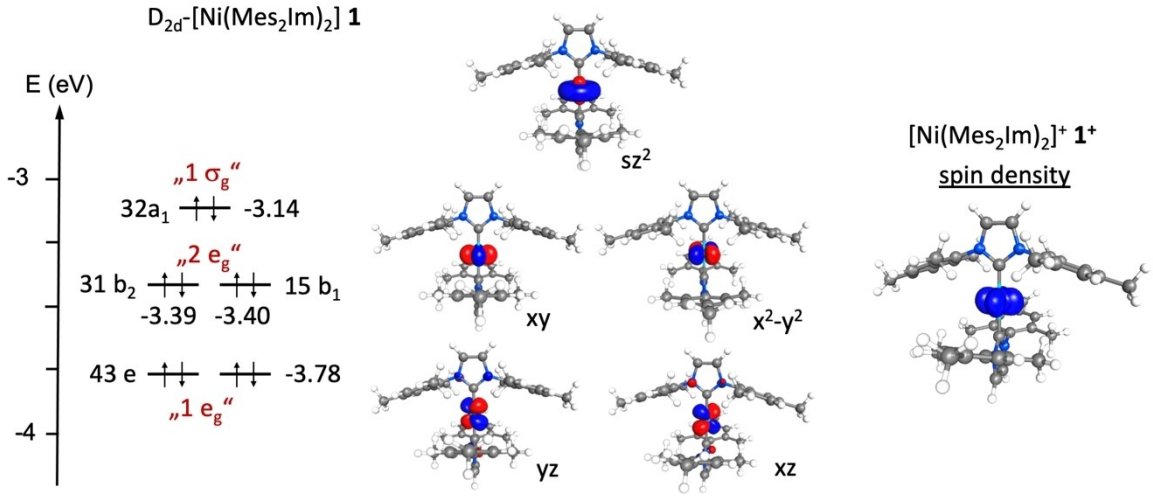

Figure 3. Highest-lying occupied molecular orbitals of $[Ni(Mes_2Im)_2]$ **1**, with associated energies (PBE0//def2-TZVP(Ni)/def2-SVP(C,N,H)). Symmetry labels given in black reflect local D_{2d} geometry, those given in red pseudo-$D_{\infty}h$ symmetry at the metal center. On the right side a plot of the DFT-calculated (PBE0//def2-TZVP(Ni)/def2-SVP(C,N,H)) spin density of $[Ni(Mes_2Im)_2]^+$ **1**$^+$ is shown.

described by a single-configuration DFT calculation. However, we also provide in Figure 3 the DFT-calculated spin density of this complex which reveals oxidation from the "$2e_g$" set of $[Ni(Mes_2Im)_2]$. Whittlesey and co-workers recently described a similar very unique orbital splitting for their six- or seven-membered $[Ni^I(NHC)_2]$ complexes **C1**–**C4** by *ab initio* ligand-field analysis (AI-LFT). They reported an orbital order of $(d_{xz}, d_{yz}) < d_z2 \approx (d_{xy}, d_x2_{-y}2)$, where the d_{xz} and d_{yz} orbitals are stabilized by π-backbonding from Ni to the NHCs and d_z2 is stabilized by 3d–4s mixing. This leads to an orbitally degenerate ground state $^2\Delta$ and a very large magnetic anisotropy. This orbital degeneracy is also central to understanding of the EPR spectra and the magnetic properties of **1**$^+$ and the analogous complexes **2**$^+$–**5**$^+$ (see below).

To probe if (reversible) one-electron oxidation is possible for all complexes **1**–**5**, cyclovoltammetry measurements were carried out on these compounds (Figure 4). The cyclic voltammograms (CV) show each the presence of a chemically

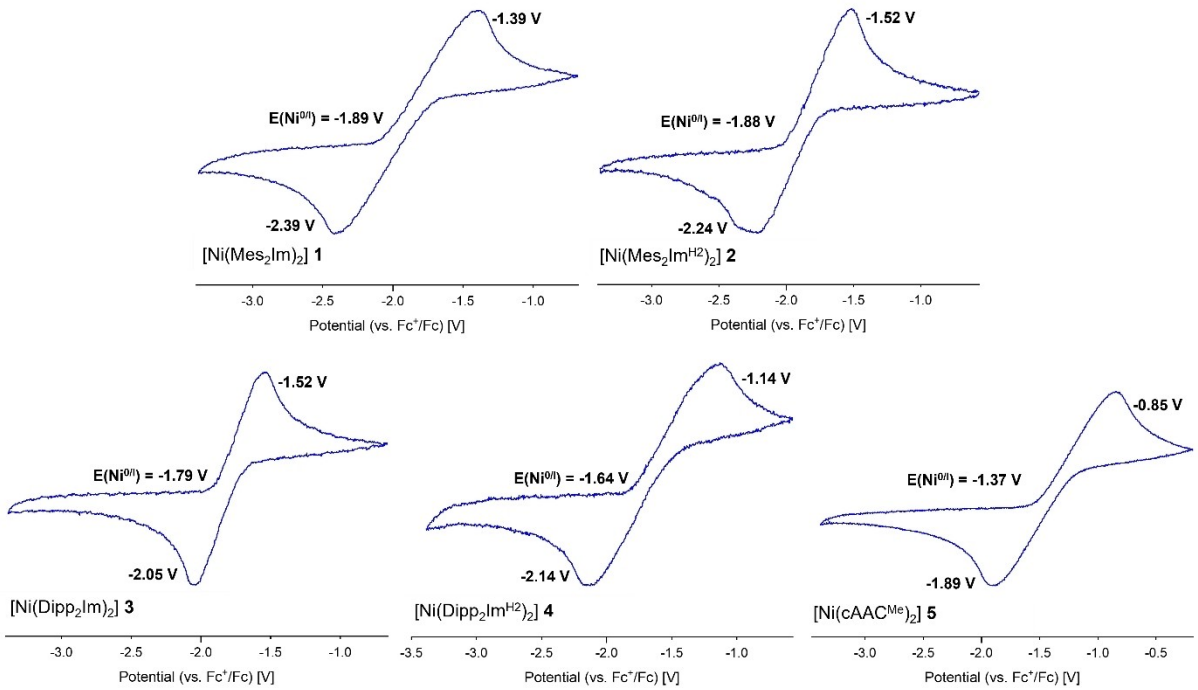

Figure 4. Cyclic voltammograms of the Ni^0/Ni^I redox couple of complexes **1**–**5** (in THF vs Fc^+/Fc).

Research Article
doi.org/10.1002/ejic.202200416

reversible oxidation/reduction associated with a redox potential between −1.89 V (**1**) and −1.37 V (**5**) for the redox couple Ni^0/Ni^I (in THF vs Fc^+/Fc).[25] All CVs revealed nearly identical oxidation potentials for the NHC complexes in a narrow range between −1.89 V and −1.64 V, whereas [Ni(cAAC^{Me})$_2$] **5** shows a significantly reduced redox potential in solution (−1.37 V), which is in line with the better accepting capabilities of the cAAC^{Me} ligand and thus reduced electron density at the central nickel atom.[26]

According to the CV spectra, one-electron oxidation using the $[FeCp_2]^+$ cation, as published previously for the synthesis of $[Ni^I(Mes_2Im)_2][BF_4]$ $\mathbf{1}^{+BF4}$, should allow synthesis and preparation of the $[Ni^I(NHC)_2]^+$ cations under consideration. However, since $\mathbf{1}^{+BF4}$ had only low solubility in common organic solvents and Ni–F contacts to the counter ion (or even a complete fluoride transfer) could not be excluded with certainty, we decided to use the tetraphenyl-borate salt $[FeCp_2][BPh_4]$ as oxidation reagent for this study. This anion should improve solubility of the corresponding nickel complex and prevent anion-cation contact to the cationic metal center. Thus, complexes $[Ni^I(Mes_2Im)_2][BPh_4]$ $\mathbf{1}^+$, $[Ni^I(Mes_2Im^{H2})_2][BPh_4]$ $\mathbf{2}^+$, $[Ni^I(Dipp_2Im)_2][BPh_4]$ $\mathbf{3}^+$, $[Ni^I(Dipp_2Im^{H2})_2][BPh_4]$ $\mathbf{4}^+$ and $[Ni^I(cAAC^{Me})_2][BPh_4]$ $\mathbf{5}^+$ were synthesized upon addition of one equiv. of $[FeCp_2][BPh_4]$ to solutions of the neutral Ni(0) compounds and isolated as colorless, off-white or yellow ($\mathbf{5}^+$) solids in good to excellent yields of 66–89% (see Scheme 1). The salts are insoluble in non-polar solvents such as hexane, toluene or benzene, $\mathbf{1}^+$–$\mathbf{4}^+$ are soluble in THF, while $\mathbf{5}^+$ is soluble in dichloromethane. The complexes were fully characterized by using elemental analysis, IR and NMR spectroscopy, HRMS and XRD. The paramagnetically shifted ^{1}H-NMR spectra of compounds $\mathbf{1}^+$–$\mathbf{5}^+$ all reveal the same number of signals as their neutral Ni(0) analogues plus three broad resonances in the aromatic region which belong to the phenyl rings of the $[BPh_4]^-$ counter ion. For example, the ^{1}H NMR spectra of $\mathbf{1}^+$ and $\mathbf{2}^+$ both reveal seven paramagnetically shifted broad resonances in the range between −3.00 ppm and 21.08 ppm with significant broadening of each signal of ca. 3–4 ppm. For the complexes $\mathbf{3}^+$ and $\mathbf{4}^+$, nine strongly shifted broad signals were detected in the range between −51.07 and 71.84 ppm, respectively. $\mathbf{5}^+$ reveals 11 signals in a range between −14.36 and 24.66 ppm in the ^{1}H-NMR spectrum. The ^{11}B-NMR spectra of each salt revealed one sharp singlet for the tetraphenyl-borate salts, with different paramagnetic shifts in the range between −6.50 and −4.15 ppm.

Crystals suitable for X-ray diffraction of compounds $\mathbf{1}^+$–$\mathbf{5}^+$ were obtained either by slow diffusion of hexane into a saturated THF solution ($\mathbf{1}^+$), slow evaporation of THF ($\mathbf{2}^+$) or DCM ($\mathbf{5}^+$) solutions of the corresponding complex, or by storing saturated solutions of the salt in THF at −30 °C ($\mathbf{3}^+$ and $\mathbf{4}^+$) (see Figure 5 and Figures S11 to S15 in the SI). The complexes crystallize in the monoclinic space groups C2/c ($\mathbf{1}^+$, $\mathbf{2}^+$ and $\mathbf{5}^+$) or $P2_1/n$ ($\mathbf{3}^+$), except for $\mathbf{4}^+$, which crystallizes in the triclinic space group $P\bar{1}$. All compounds $\mathbf{1}^+$–$\mathbf{5}^+$ reveal linear geometries with $C_{carbene}$–Ni–$C_{carbene}$ angles in the range between 178.27(7)° and 180° and Ni–$C_{carbene}$ distances of 1.8954(12)–1.9779(16) Å. In each case, the Ni–$C_{carbene}$ bond lengths are slightly longer compared to their neutral analogues **1**–**5** (see Table 1), as predicted by the DFT-calculations (*vide supra*).[19–22] With this elongation of the nickel-carbene bond in the radical cations comes an increase in the N–C–N angle of the coordinated carbene, which corresponds to an increased p-character in the carbene σ-type orbitals due to the polarization of the Ni–C bonds of the cations towards the metal center. The torsion angles between the NHC or cAAC^{Me} ligands, spanned by the two planes N–$C_{carbene}$–N or N–$C_{carbene}$–CMe_2 (for $\mathbf{5}^+$), which were observed in the range of 0°–53° do not follow a simple trend. The cAAC^{Me} complex $\mathbf{5}^+$ reveals no twisting between the cAAC^{Me} ligands (compared to 60.7° in the neutral complex **5**) while the torsion angles of $\mathbf{1}^+$ and $\mathbf{2}^+$ strongly decrease and the torsion angles of $\mathbf{3}^+$ and $\mathbf{4}^+$ just slightly increase upon oxidation.

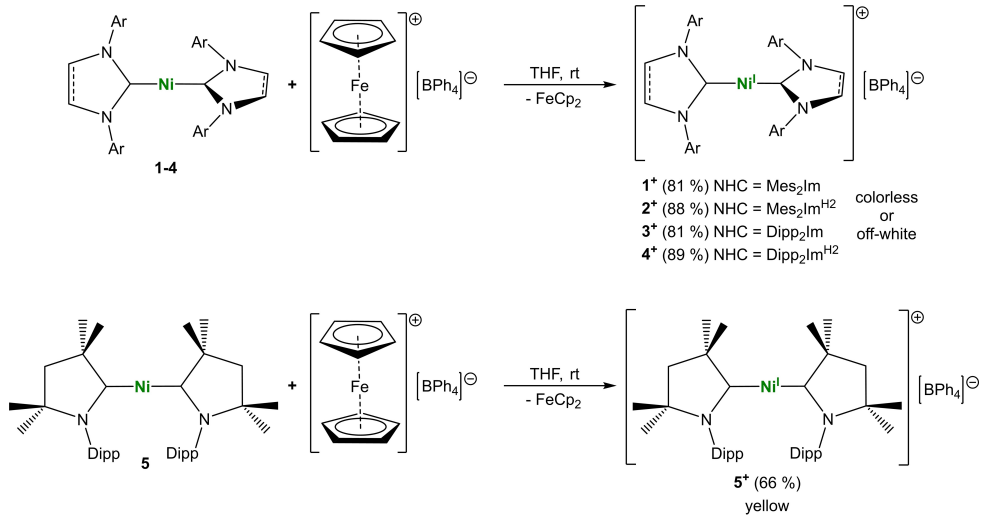

Scheme 1. Synthesis of linear Ni(I) complex cations of $[Ni^I(Mes_2Im)_2][BPh_4]$ $\mathbf{1}^+$, $[Ni^I(Mes_2Im^{H2})_2][BPh_4]$ $\mathbf{2}^+$, $[Ni^I(Dipp_2Im)_2][BPh_4]$ $\mathbf{3}^+$, $[Ni^I(Dipp_2Im^{H2})_2][BPh_4]$ $\mathbf{4}^+$ and $[Ni^I(cAAC^{Me})_2][BPh_4]$ $\mathbf{5}^+$.

Research Article
doi.org/10.1002/ejic.202200416

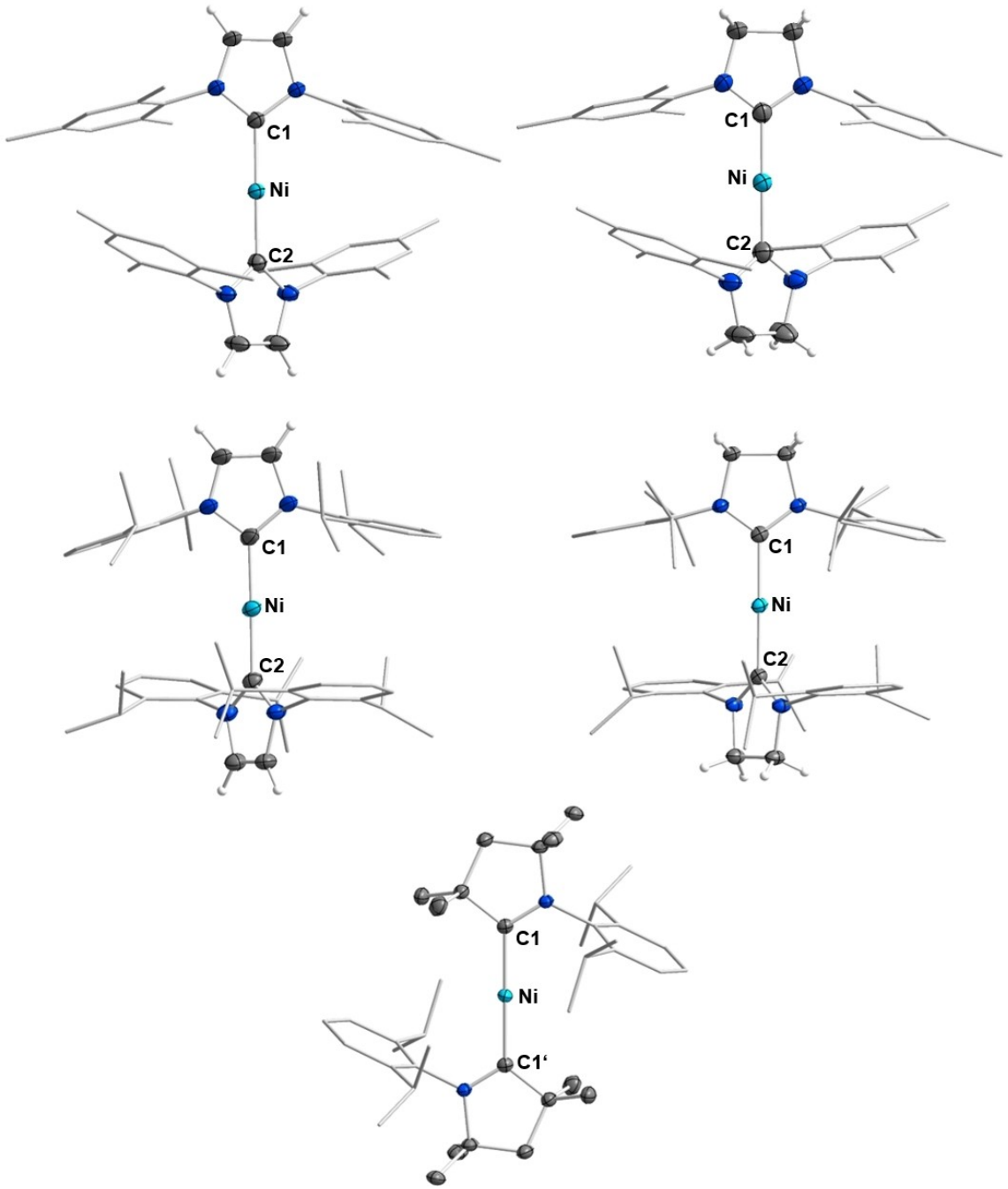

Figure 5. Molecular structures of the cations of $[Ni^{I}(NHC)_2][BPh_4]$: $[Ni^{I}(Mes_2Im)_2]^+$ of $\mathbf{1}^+$ (top left), $[Ni^{I}(Mes_2Im^{H2})_2]^+$ of $\mathbf{2}^+$ (top right), $[Ni^{I}(Dipp_2Im)_2]^+$ of $\mathbf{3}^+$ (middle left), $[Ni^{I}(Dipp_2Im^{H2})_2]^+$ of $\mathbf{4}^+$ (middle right) and $[Ni^{I}(cAAC^{Me})_2]^+$ of $\mathbf{5}^+$ (bottom center) in the solid state (ellipsoids set at the 50 % probability level). The BPh_4 anions, co-crystallized THF molecules ($\mathbf{3}^+$ and $\mathbf{4}^+$) and hydrogen atoms, except of the backbone hydrogen atoms have been omitted for clarity. For selected bond lengths [Å] and angles [°] of $\mathbf{1}^+$–$\mathbf{5}^+$ see Table 1 and Figures S11-S15 in the Supporting Information.

Measurements of the magnetic moments μ_{eff} in solution of compounds $\mathbf{1}^+$–$\mathbf{5}^+$ (Evans method) in THF-d_8 or CD_2Cl_2 ($\mathbf{5}^+$) revealed values between 2.26–3.15 μ_B. All values are significantly larger than the spin-only value of 1.73 μ_B, but also differ certainly from the values of 3.0–3.3 μ_B observed for linear complexes $[Ni^{I}(NHC)_2]^+$ **C1**–**C4** stabilized by six- and seven-membered NHC ligands.[18] To get further insight into the magnetic properties of $\mathbf{1}^+$–$\mathbf{5}^+$ EPR experiments were performed on frozen solutions of each of the complexes ($\mathbf{1}^+$–$\mathbf{4}^+$ in THF and $\mathbf{5}^+$ in DCM) as well as on polycrystalline powder samples (compare Table 2 and Figure 6). The powder spectra of $\mathbf{1}^+$–$\mathbf{4}^+$ revealed highly anisotropic *g*-tensors, with g_1 values between 5.09–5.77, as it was observed previously for comparable compounds (**C1**–**C4**).[18] In contrast to Whittlesey's complexes **C1**–**C4**, the five-ring NHC complex cations produced very different g_2 and g_3 values, depending on the carbene. In

Research Article
doi.org/10.1002/ejic.202200416

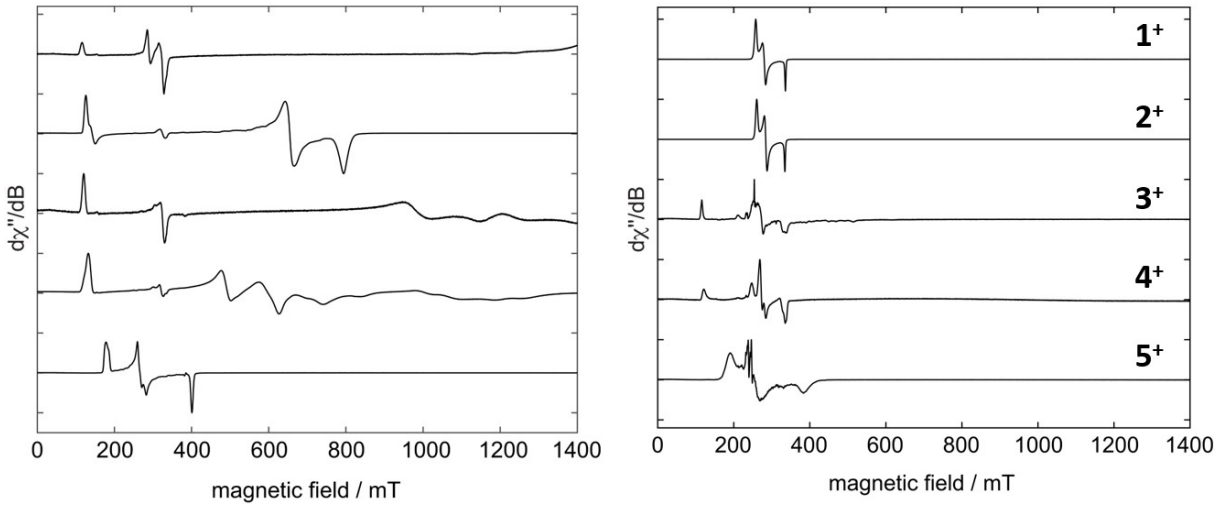

Figure 6. Experimental powder X-band CW-EPR spectra of $\mathbf{1}^+$–$\mathbf{5}^+$ (left) and in frozen solution at 10 K (right, $\mathbf{1}^+$–$\mathbf{4}^+$ in THF and $\mathbf{5}^+$ in DCM). For $\mathbf{1}^+$–$\mathbf{4}^+$ the signals in the region of 200–400 mT are attributed to paramagnetic impurities or solvent adducts. For detailed experimental conditions and simulation parameters see Figures S21–S32 in the Supporting Information.

general, the complexes bearing NHCs with saturated backbones ($\mathbf{2}^+$: $g_2 = 1.02$, $g_3 = 0.84$ and $\mathbf{4}^+$: $g_2 = 1.37$, $g_3 = 1.07$) revealed higher g_2 and g_3 values than their counterparts with unsaturated NHC-backbones ($\mathbf{1}^+$: $g_2 \sim 0.46$, $g_3 =$ outside the range of the magnetic field and $\mathbf{3}^+$: $g_2 = 0.68$, $g_3 = 0.58$) and the *N*-Dipp substituted carbenes led to higher g_2/g_3 values compared to the *N*-Mes substituted NHCs. Thus, we found the most extreme *g*-tensor anisotropy for compound $\mathbf{1}^+$ ($g_1 = 5.77$, $g_2 \sim 0.46$, $g_3 =$ outside the range of the magnetic field), which is in the same region as reported for the complexes **C1**–**C4** ($g_1 = 5.66$–5.89, $g_2 = 0.56$–0.62, $g_3 = 0.55$–0.58).[18] For the cAAC^{Me} stabilized complex $\mathbf{5}^+$ *g*-tensors which are much less anisotropic ($g_1 = 3.73$, $g_2 = 2.50$, $g_3 = 1.67$) were observed.

Interestingly, the solution EPR spectra of $\mathbf{1}^+$–$\mathbf{4}^+$ differ considerably from the powder spectra. For the *N*-Mes substituted compounds $\mathbf{1}^+$ and $\mathbf{2}^+$, the EPR spectra measured in THF solutions showed completely new species with *g*-values between 2.60 and 2.00, which are clearly not caused by a linear complex.[9,17] For *N*-Dipp substituted $\mathbf{3}^+$ and $\mathbf{4}^+$ only the g_1 values could be resolved with a much smaller intensity and some new signals between 200 and 400 mT, arising from impurities or solvent adducts. Interestingly, we obtained a second crystal structure for the complex [Ni^{I}(Mes$_2$Im)$_2$][BF$_4$] $\mathbf{1}^{+\,BF4}$ published previously, in which the unit cell contains different cations, of which two-thirds are coordinated by an additional THF molecule (Figure 7). This finding is a likely explanation for the EPR resonances found for *N*-Mes substituted complexes $\mathbf{1}^+$ and $\mathbf{2}^+$ in solution, which indicate a non-linear geometry. The resulting signals presumably originate from a T-shaped solvent (THF) adduct formed in solution. For $\mathbf{3}^+$ and $\mathbf{4}^+$ adduct formation is less likely due to the increased steric protection of the nickel atom using the larger *N*-Dipp substituted NHC ligands.

Table 2. Experimental *g*-Tensors of the powder samples of $\mathbf{1}^+$–$\mathbf{5}^+$ and in solution (shown in parentheses).

Compound	g_1	g_2	g_3
[Ni^{I}(Mes$_2$Im)$_2$][BPh$_4$] $\mathbf{1}^+$	5.77 (2.60)	0.46 (2.39)	−(2.00)
[Ni^{I}(Mes$_2$Im^{H2})$_2$][BPh$_4$] $\mathbf{2}^+$	5.32 (2.58)	1.02 (2.36)	0.84 (2.01)
[Ni^{I}(Dipp$_2$Im)$_2$][BPh$_4$] $\mathbf{3}^+$	5.58 (5.78)	0.68 (–)	0.58 (–)
[Ni^{I}(Dipp$_2$Im^{H2})$_2$][BPh$_4$] $\mathbf{4}^+$	5.09 (5.53)	1.37 (–)	1.07 (–)
[Ni^{I}(cAAC^{Me})$_2$][BPh$_4$] $\mathbf{5}^+$	3.73	2.50	1.67

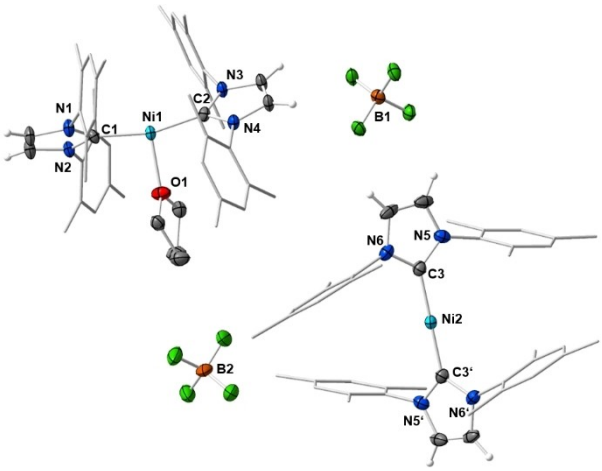

Figure 7. Molecular structures of [Ni^{I}(Mes$_2$Im)$_2$(THF)][BF$_4$] $\mathbf{1}^{+THF}$ and [Ni^{I}-(Mes$_2$Im)$_2$][BF$_4$] $\mathbf{1}^{+BF4}$ in the solid state (ellipsoids set at the 50% probability level). All hydrogen atoms except of the backbone hydrogen atoms have been omitted for clarity. Selected bond lengths [Å] and angles [°] of $\mathbf{1}^{+THF}$: Ni1–C1 1.939(3), Ni1–C2 1.939(3), Ni1–O1 2.094(2), C1–N1 1.362(4), C1–N2 1.365(4), C2–N3 1.365(4), C2–N4 1.358(4); C1–Ni1–C2 164.13(14), C1–Ni1-O1 97.01(12), C2–Ni1–O1 98.86(12), plane (N1–C1–N2) – plane (N3–C2–N4) 54.72(14).Selected bond lengths [Å] and angles [°] of $\mathbf{1}^{+BF4}$: Ni2–C3 1.891(3), C3–N5 1.363(4), C3–N6 1.364(4), C3–Ni2–C3′ 179.8(2), N5–C3–N6 103.7(3), plane (N5–C3–N6) – plane (N5′–C3′–N6′) 59.27(13).

Conclusion

It has been demonstrated previously that homoleptic two-coordinated, linear Ni(I) complexes possess very interesting properties, which allow different applications in small molecule activation, catalysis and magnetism. We demonstrate here that redox processes in complexes [Ni(NHC)$_2$], often used in catalysis, easily occur. The redox potentials for a reversible oxidation/reduction process for the redox couple Ni^0/Ni^I lies for the complexes [Ni(Mes$_2$Im)$_2$] **1**, [Ni(Mes$_2$Im^{H2})$_2$] **2**, [Ni(Dipp$_2$Im)$_2$] **3** and [Ni(Dipp$_2$Im^{H2})$_2$] **4** in THF vs Fc^+/Fc in a narrow range between −1.89 (**1**) V and −1.64 V (**4**), depending on the NHC used. [Ni(cAAC^{Me})$_2$] **5** shows a significantly reduced redox potential in solution (-1.37 V), which is in line with the better accepting capabilities of the cAAC^{Me} ligand. Due to the excellent steric protection provided by the NHC ligand and the low lying oxidation potential we believe that electron transfer processes are much more important in catalytic systems using [Ni(NHC)$_2$] as a catalysts as generally accepted. We have used this low lying one-electron oxidation process for the synthesis of a variety of stable, two-coordinate nickel-d^9 complexes [Ni^I(NHC)$_2$]$^+$, stabilized by classical five-ring Arduengo-carbenes and a cyclic (alkyl)(amino)carbene (cAAC). Isolation of the complexes [Ni^I(Mes$_2$Im)$_2$][BPh$_4$] **1**$^+$, [Ni^I(Mes$_2$Im^{H2})$_2$][BPh$_4$] **2**$^+$, [Ni^I(Dipp$_2$Im)$_2$][BPh$_4$] **3**$^+$, [Ni^I(Dipp$_2$Im^{H2})$_2$][BPh$_4$] **4**$^+$ and [Ni^I(cAAC^{Me})$_2$][BPh$_4$] **5**$^+$ was achieved by one-electron oxidation of the corresponding linear Ni(0) complexes, using ferrocenium tetraphenyl-borate as oxidizing reagent. X-ray diffraction studies of **1**$^+$–**5**$^+$ revealed linear geometries and the paramagnetic nature of the complexes was verified by NMR measurements, measurement of the magnetic moments in solution (Evans' method, range between 2.26–3.15 μ_B) and EPR spectroscopy. DFT calculations performed on [Ni(Mes$_2$Im)$_2$] **1** and [Ni(Mes$_2$Im)$_2$]$^+$ **1**$^+$ predicted that oxidation occurs from a degenerate e_g set of orbitals, leading to an orbitally degenerate ground state and thus to large magnetic anisotropy in complex **1**$^+$. Theory was confirmed by EPR experiments, showing very high magnetic anisotropies in the solid state for the compounds **1**$^+$–**4**$^+$, while the cAAC^{Me}-stabilized complex **5**$^+$ revealed significantly reduced anisotropical *g*-tensors. Additional EPR measurements in solution demonstrated extreme variations of the magnetic properties of **1**$^+$–**4**$^+$, which culminated in a noticeable decrease of the *g*-tensor anisotropy for the *N*-Mes substituted complexes **1**$^+$ and **2**$^+$ in solution. This behavior is most likely due to the formation of T-shaped solvent (THF) adducts, which was exemplified by the observed crystal structure of [Ni^I(Mes$_2$Im)$_2$(THF)][BF$_4$] **1**$^{+THF}$. This study once again illustrates the strong influence of the steric protection by a ligand to the complex metal center with respect to its stability and its magnetic behavior.

Experimental Section

General

All reactions and subsequent manipulations were performed under an argon atmosphere using standard Schlenk techniques as reported previously[27] or in a glovebox (Innovative Technology Inc. or Braun Uni Lab). All reactions were carried out in oven-dried glassware. Toluene, benzene, hexane and THF were purified by distillation from an appropriate drying agent (sodium with benzophenone as indicator). $CDCl_3$, C_6D_6 and THF-d_8 was purchased from Sigma-Aldrich. [Ni(η^4-COD)$_2$],[28] the NHCs (Mes$_2$Im, Mes$_2$Im^{H2}, Dipp$_2$Im, Dipp$_2$Im^{H2}[29] and cAAC^{Me}[30]) and [FeCp$_2$][BPh$_4$][31] were prepared according to published procedures. [$NiBr_2$·DME] was prepared from the bromination of nickel in DME. All other reagents were purchased from Aldrich or ABCR and used without further purification. NMR spectra were recorded at 298 K using Bruker Avance 400 (^{1}H, 400 MHz; ^{13}C, 100 MHz; ^{11}B, 128 MHz; ^{19}F, 376 MHz; ^{31}P, 162 MHz, ^{29}Si, 79.5 MHz), or Bruker Avance NEO 400 (^{1}H, 400 MHz; ^{13}C, 100 MHz; ^{11}B, 128 MHz; ^{19}F, 376 MHz; ^{31}P, 162 MHz; ^{29}Si, 79.5 MHz), or Bruker Avance 500 (^{1}H, 500 MHz; ^{13}C, 126 MHz; ^{11}B, 160 MHz) spectrometers. ^{1}H NMR chemical shifts are reported relative to TMS and were referenced via residual proton resonances of the corresponding deuterated solvent ($CDCl_3$: 7.26 ppm, C_6D_5H: 7.16 ppm, THF-d_8: 3.58/1.72 ppm) whereas $^{13}C\{^1H\}$ NMR spectra are reported relative to TMS using the natural-abundance carbon resonances ($CDCl_3$: 77.16 ppm, C_6D_6: 128.06 ppm, THF-d_8: 67.21/25.31 ppm). Coupling constants are given in Hertz. Elemental analyses were performed in the microanalytical laboratory of the Institute of Inorganic Chemistry, Universität Würzburg, using an Elementar vario micro cube. High-resolution mass spectra were obtained using a Thermo Scientific Exactive Plus spectrometer equipped with an Orbitrap Mass Analyzer. Ionizations were accomplished in Liquid Injection Field Desorption Ionization mode using a LIFDI 700 from Linden CMS with 10 kV at the emitter and an accelerating voltage of 5 V. Cyclic voltammetry experiments were performed using a PINE Instruments AFCBP1 bipotentiostat with a commercially available cell (ALS Co. Ltd., VC-4) in an argon filled glovebox. Commercial glassy carbon disk electrodes (2 mm diameter, BaSi) and platinum wire (0.4 mm × 5.7 mm, ALS Co. Ltd.) counter electrodes, as well as commercial silver wire reference electrodes (RE-7, ALS Co. Ltd.), separated from the main compartment by ion permeable porous glass and filled with a 0.01 M $AgNO_3$ stock solution in acetonitrile, were used. Measurements were performed in argon purged THF using 0.1 M [TBA][PF_6] (bought from Fluka, 98 + %) as supporting electrolyte. Potentials are referenced to the ferrocene/ferrocenium couple.[24] EPR measurements at X-band (9.38 GHz) were carried out using a Bruker ELEXSYS E580 CW EPR spectrometer equipped with an Oxford Instruments helium cryostat (ESR900) and a MercuryiTC temperature controller. The spectral simulations were performed using MATLAB 9.11.0 (R2021b) and the EasySpin 5.2.33 toolbox.[32]

The NHCs (Mes$_2$Im, Mes$_2$Im^{H2}, Dipp$_2$Im, Dipp$_2$Im^{H2} and cAAC^{Me}) and [FeCp$_2$][BPh$_4$] were synthesized according to literature procedures.[29–31]

Synthesis

[Ni(Mes$_2$Im)$_2$] 1 and [Ni(Mes$_2$Im^{H2})$_2$] 2

[Ni(Mes$_2$Im)$_2$] **1** and [Ni(Mes$_2$Im^{H2})$_2$] **2** were prepared by a slightly modified literature procedure.[19–20]

A solution of the NHC (2 equiv., NHC=Mes$_2$Im or Mes$_2$Im^{H2}) in THF was added at room temperature to a solution of [Ni(η^4-COD)$_2$]

Research Article
doi.org/10.1002/ejic.202200416

(1 equiv., batch sizes ca. 1.00 g) in THF. The dark purple reaction mixture was stirred for 24 h at room temperature and was than filtered over a pad of celite. All volatiles were removed in vacuo and the remaining residue was suspended in hexane. The product was filtered off and dried in vacuo to give a dark black crystalline solid (Yield: 80% (**1**), 63% (**2**)). The spectroscopic data of **1** and **2** match those reported in the literature.[19–20]

Black crystals of $Ni(Mes_2Im^{H2})_2$ **2** suitable for single-crystal X-ray diffraction were obtained from storing a saturated solution in hexane at −30 °C.

[Ni(Dipp$_2$Im)$_2$] 3, [Ni(Dipp$_2$Im^{H2})$_2$] 4 and [Ni(cAAC^{Me})$_2$] 5

$[Ni(Dipp_2Im)_2]$ **3**, $[Ni(Dipp_2Im^{H2})_2]$ **4** and $[Ni(cAAC^{Me})_2]$ **5** were prepared by slightly modified literature procedures[20–22,33] starting from $[NiBr_2 \cdot DME]$.

A solution of the NHC (2.1 equiv., NHC=$Dipp_2Im$, $Dipp_2Im^{H2}$, $cAAC^{Me}$) in benzene was added at room temperature to a suspension of $[NiBr_2 \cdot DME]$ (1 equiv., batch sizes ca. 1.00 g) in benzene. The reaction mixture was stirred for 24 h at room temperature and was than filtered over a pad of celite. All volatiles were removed in vacuo and the remaining residue was suspended in hexane. The precipitate was filtered off and dried in vacuo to give the intermediate complex $[Ni(NHC)_2Br_2]$ as pink powder (Yield: 69% ($cAAC^{Me}$), 81% ($Dipp_2Im$), 98% ($Dipp_2Im^{H2}$).

$[Ni(NHC)_2Br_2]$ (1 equiv.) and KC_8 (3.1 equiv.) were suspended in THF. The dark purple reaction mixture was stirred for 24 h at room temperature and was than filtered over a pad of celite. All volatiles were removed in vacuo and the remaining residue was redissolved in toluene and then again filtered over a pad of celite. The solvent was removed in vacuo and the product was suspended in hexane, filtered, and dried in vacuo to give a dark black crystalline solid (Yield: 62% (**3**) 68% (**4**), 43% (**5**)). The spectroscopic data of **3**, **4** and **5** match those reported in the literature.[21a,22]

[FeCp$_2$][BPh$_4$][31]

Ferrocene (1.50 g, 8.06 mmol) was dissolved in 30 mL of concentrated sulfuric acid and stirred for 30 min at room temperature. The blue solution was then poured into 300 mL of water and a solution of sodium tetraphenylborate (3.28 g, 9.59 mmol) in 150 mL of water was added. The mixture was then stirred for 2 h at room temperature whereby a light blue precipitate was formed. The product was filtered off and washed with 300 mL of water, 100 mL of ethanol and 150 mL of diethylether, successively. The product was dried in vacuo to give a light blue powder (3.3 g, 6.53 mmol, 81%).

[Ni^{I}(Mes$_2$Im)$_2$][BPh$_4$] 1$^+$

$[Ni(Mes_2Im)_2]$ (200 mg, 300 μmol) and ferrocenium tetraphenylborate (151 mg, 300 μmol) were dissolved in 10 mL of THF. The reaction mixture was stirred for 2 h at room temperature and was then filtered over a pad of celite. All volatiles of the resulting solution were removed in vacuo and the remaining residue was suspended in 5 mL of hexane. The product was filtered off, washed with 5 mL of benzene and again with 15 mL of hexane. The product was dried in vacuo to give an off-white powder (240 mg, 243 μmol, 81%).

Colorless crystals of $[Ni^{I}(Mes_2Im)_2][BPh_4]$ **1**$^+$ suitable for single-crystal X-ray diffraction were obtained by slow diffusion of hexane into a saturated THF solution of.

Elemental analysis $C_{66}H_{68}BN_4Ni$ [986.80 g/mol] calculated (found): C 80.33 (79.58), H 6.95 (7.04), N 5.68 (5.79).

HRMS-LIFDI m/z (%) calculated for $[C_{42}H_{48}N_4Ni]^+$: 666.3233(100) $[M]^+$; found: 666.3213(100) $[M]^+$, 305.2006(10) $[Mes_2Im+H]^+$.

^{1}H-NMR (400.1 MHz, THF-d_8, 298 K): δ = 0–2.5 (vbr, s), 1.31 (br, s), 4.81 (br, s), 6.76 (br, s, 4H, $B(C_6H_5)_4$), 6.93 (br, s, 8H, $B(C_6H_5)_4$), 7.47 (br, s, 8H, $B(C_6H_5)_4$), 17.87 (vbr, s).

^{11}B-NMR (128.5 MHz, THF-d_8, 298 K): $\delta = -6.32$ (s, 1B, BPh_4).

IR (ATR [cm^{-1}]): 3122 (vw), 3054 (vw), 2913 (vw), 1579 (vw), 1484 (w), 1406 (vw), 1377 (vw), 1334 (vw), 1241 (w), 1031 (w), 925 (vw), 850 (m), 741 (m), 729 (m), 705 (vs), 612 (m), 573 (w), 475 (vw), 435 (vw).

Magnetic moment (Evans): μ_{eff} (THF-d_8, 298 K) = 2.42 μ_B

[Ni^{I}(Mes$_2$Im^{H2})$_2$][BPh$_4$] 2$^+$

$[Ni(Mes_2Im^{H2})_2]$ (200 mg, 298 μmol) and ferrocenium tetraphenylborate (150 mg, 298 μmol) were dissolved in 10 mL of THF. The reaction mixture was stirred for 2 h at room temperature and was then filtered over a pad of celite. All volatiles of the resulting solution were removed in vacuo and the remaining residue was suspended in 5 mL of benzene. The product was filtered off, washed with 5 mL of benzene and with 15 mL of hexane. The product was dried in vacuo to give a colorless powder (260 mg, 262 μmol, 88%).

Colorless crystals of $[Ni^{I}(Mes_2Im^{H2})_2][BPh_4]$ **2**$^+$ suitable for single-crystal X-ray diffraction were obtained by slow evaporation of a saturated THF solution.

Elemental analysis $C_{66}H_{72}BN_4Ni$ [990.83 g/mol] calculated (found): C 80.01 (79.99), H 7.32 (7.46), N 5.65 (5.53).

HRMS-LIFDI m/z (%) calculated for $[C_{42}H_{52}N_4Ni]^+$: 670.3546(100) $[M]^+$; found: 670.3529(60) $[M]^+$, 307.2162(10) $[Mes_2Im^{H2}+H]^+$.

^{1}H-NMR (400.1 MHz, THF-d_8, 298 K): $\delta = -3.0$–0.5 (vbr, s), −0.62 (br, s), 0.76 (br, s), 7.15 (br, s, 4H, $B(C_6H_5)_4$), 7.43 (br, s, 8H, $B(C_6H_5)_4$), 8.25 (br, s, 8H, $B(C_6H_5)_4$), 21.08 (vbr, s).

^{11}B-NMR (128.5 MHz, THF-d_8, 298 K): $\delta = -5.47$ (s, 1B, BPh_4).

IR (ATR [cm^{-1}]): 3055 (w), 3033 (w), 2998 (vw), 2981 (w), 2911 (w), 2852 (vw), 1609 (vw), 1579 (vw), 1487 (s), 1453 (m), 1425 (m), 1374 (w), 1319(w), 1299 (w), 1266 (s), 1178 (w), 1133 (w), 1067 (vw), 1030 (m), 1011 (w), 916 (vw), 848 (m), 811 (w), 743 (m), 739 (s), 705 (vs), 682 (w), 612 (s), 571 (m), 529 (vw), 500 (vw), 464 (w), 425 (w).

Magnetic moment (Evans): μ_{eff} (THF-d_8, 298 K) = 2.49 μ_B

[Ni^{I}(Dipp$_2$Im)$_2$][BPh$_4$] 3$^+$

$[Ni(Dipp_2Im)_2]$ (190 mg, 227 μmol) and ferrocenium tetraphenylborate (115 mg, 227 μmol) were dissolved in 10 mL of THF. The reaction mixture was stirred for 2 h at room temperature and was then filtered over a pad of celite. All volatiles of the resulting solution were removed in vacuo and the remaining residue was suspended in 5 mL of benzene. The product was filtered off, washed with 5 mL of benzene and with 15 mL of hexane. The product was dried in vacuo to give a colorless powder (211 mg, 183 μmol, 81%).

Colorless crystals of $[Ni^{I}(Dipp_2Im)_2][BPh_4]$ **3**$^+$ suitable for single-crystal X-ray diffraction were obtained from storing a saturated solution in THF at −30 °C.

Elemental analysis $C_{78}H_{92}BN_4Ni$ [1155.13 g/mol] calculated (found): C 81.10 (80.51), H 8.03 (8.02), N 4.85 (4.74).

HRMS-LIFDI m/z (%) calculated for $[C_{54}H_{72}N_4Ni]^+$: 834.5111(100) $[M]^+$; found: 834.5095(40) $[M]^+$, 389.2948(100) $[Dipp_2Im+H]^+$.

^{1}H-NMR (400.1 MHz, THF-d_8, 298 K): $\delta=-51.07$(vbr, s), −11.57 (br, s), −8.71 (br, s) 7.10 (br, s, 4H, $B(C_6H_5)_4$), 7.50 (br, s, 8H, $B(C_6H_5)_4$), 8.18 (br, s), 8.52 (br, s, 8H, $B(C_6H_5)_4$), 37.24 (vbr, s), 71.84 (vbr, s).

^{11}B-NMR (128.5 MHz, THF-d_8, 298 K): $\delta=-5.15$ (s, 1B, BPh_4).

IR (ATR [cm^{-1}]): 3150 (vw), 3054 (vw), 2962 (w), 2926 (vw), 2868 (vw), 1580 (vw), 1561 (vw), 1460 (m), 1425 (vw), 1399 (w), 1385 (vw), 1364 (w), 1327 (w), 1270 (vw), 1211 (vw), 1181 (vw), 1107 (vw), 1061 (w), 1032 (vw), 940 (w), 842 (vw), 802 (m), 758 (s), 746 (m), 731 (s), 703 (vs), 612 (s), 551 (vw), 469 (w), 454 (w).

Magnetic moment (Evans): μ_{eff} (THF-d_8, 298 K) = 3.15 μ_B

$[Ni^I(Dipp_2Im^{H2})_2][BPh_4]$ 4$^+$

$[Ni(Dipp_2Im^{H2})_2]$ (200 mg, 238 μmol) and ferrocenium tetraphenylborate (120 mg, 238 μmol) were dissolved in 10 mL of THF. The reaction mixture was stirred for 2 h at room temperature and was then filtered over a pad of celite. All volatiles of the resulting solution were removed in vacuo and the remaining residue was suspended in 5 mL of benzene. The product was filtered off, washed with 5 mL of benzene and with 15 mL of hexane. The product was dried in vacuo to give a colorless powder (245 mg, 211 μmol, 89 %).

Colorless crystals of $[Ni^I(Dipp_2Im^{H2})_2][BPh_4]$ **4$^+$** suitable for single-crystal X-ray diffraction were obtained from storing a saturated solution in THF at −30 °C.

Elemental analysis $C_{78}H_{96}BN_4Ni$ [1159.16 g/mol] calculated (found): C 80.82 (80.62), H 8.35 (8.65), N 4.83 (4.62).

HRMS-LIFDI m/z (%) calculated for $[C_{54}H_{76}N_4Ni]^+$: 838.5424(100) $[M]^+$; found: 838.5399(10) $[M]^+$, 391.3097(100) $[Dipp_2Im^{H2}+H]^+$.

^{1}H-NMR (400.1 MHz, THF-d_8, 298 K): $\delta=-48.19$ (vbr, s), −9.21 (br, s), −7.23 (br, s), 6.01 (br, s), 7.74 (br, s, 4H, $B(C_6H_5)_4$), 8.26 (br, s, 8H, $B(C_6H_5)_4$), 9.49 (br, s, 8H, $B(C_6H_5)_4$), 36.71 (vbr, s), 59.96 (vbr, s).

^{11}B-NMR (128.5 MHz, THF-d_8, 298 K): $\delta=-4.15$ (s, 1B, BPh_4).

IR (ATR [cm^{-1}]): 3053 (w), 2962 (m), 2926 (w), 2869 (w), 1580 (vw), 1472 (m), 1455 (s), 1425 (m), 1384 (w), 1363 (w), 1324 (w), 1270 (s), 1242 (w), 1180 (w), 1133 (vw), 1103 (vw), 1058 (w), 1032 (w), 995 (vw), 936 (vw), 907 (vw), 842 (w), 804 (m), 759 (m), 746 (w), 731 (s), 703 (vs), 680 (m), 611 (s), 574 (vw), 549 (w), 506 (vw), 467 (w), 450 (m), 424 (w).

Magnetic moment (Evans): μ_{eff} (THF-d_8, 298 K) = 2.26 μ_B

$[Ni^I(cAAC^{Me})_2][BPh_4]$ 5$^+$

$[Ni(cAAC^{Me})_2]$ (60.0 mg, 95.3 μmol) and ferrocenium tetraphenylborate (48.2 mg, 95.3 μmol) were dissolved in 6 mL of THF. The reaction mixture was stirred for 2 h at room temperature whereby a yellow precipitate was formed. The product was filtered off, washed with 3 mL of THF and with 15 mL of hexane. The product was dried in vacuo to give a yellow powder (60 mg, 63.2 μmol, 66 %).

Yellow crystals of $[Ni^I(cAAC^{Me})_2][BPh_4]$ **5$^+$** suitable for single-crystal X-ray diffraction were obtained by slow evaporation of a saturated DCM solution.

Elemental analysis $C_{64}H_{82}BN_2Ni$ [948.88 g/mol] calculated (found): C 81.01 (80.90), H 8.71 (8.77), N 2.95 (2.88).

HRMS-LIFDI m/z (%) calculated for $[C_{40}H_{62}N_2Ni]^+$: 628.4266(100) $[M]^+$; found: 628.4254(10) $[M]^+$; 320.2134 $[cAAC^{Me}\text{-}Cl]^+$.

^{1}H-NMR (400.1 MHz, CD_2Cl_2, 298 K): $\delta=-14.36$ (vbr, s), −8.11 (br, s), −6.97 (vbr, s), 0.09 (br, s), 1.27 (vbr, s), 6.89 (br, s, 4H, $B(C_6H_5)_4$), 7.06 (br, s, 8H, $B(C_6H_5)_4$), 7.39 (br, s, 8H, $B(C_6H_5)_4$), 14.56 (vbr, s), 20.13 (vbr, s), 24.66 (vbr, s).

^{11}B-NMR (128.5 MHz, CD_2Cl_2, 298 K): $\delta=-6.50$ (s, 1B, BPh_4).

IR (ATR [cm^{-1}]): 3053 (vw), 3032 (vw), 2967 (w), 2946 (w), 2857 (vw), 1579 (w), 1498 (m), 1456 (m), 1424 (w), 1386 (w), 1370 (w), 1362 (w), 1344 (w), 1328 (w), 1265 (w), 1208 (w), 1179 (w), 1129 (m), 1112 (w), 1064 (w), 1053 (w), 1032 (w), 1001 (w), 968 (vw), 934 (vw), 846 (w), 809 (m), 780 (w), 748 (m), 737 (s), 729 (s), 703 (vs), 612 (s), 570 (w), 559 (vw), 489 (w), 475 (w), 465 (vw), 449 (w), 420 (w).

Magnetic moment (Evans): μ_{eff} (CD_2Cl_2, 298 K) = 2.82 μ_B

Crystallographic Details

Crystals were immersed in a film of perfluoropolyether oil on a glass fiber MicroMount™ (MiTeGen) and transferred to a Rigaku XtaLAB Synergy-DW diffractometer with HyPix-6000HE detector and monochromated Cu-K_α equipped with an Oxford Cryo 800 cooling unit. Data were collected at 100 K. The images were processed with the Crysalis software packages and equivalent reflections were merged. Corrections for Lorentz-polarization effects and absorption were performed if necessary and the structures were solved by direct methods. Subsequent difference Fourier syntheses revealed the positions of all other non-hydrogen atoms. The structures were solved by using the ShelXTL software package.[34] All non-hydrogen atoms were refined anisotropically. Hydrogen atoms were usually assigned to idealized positions and were included in structure factors calculations.

Crystal data for 2: $C_{42}H_{52}N_4Ni$, $M_r=671.58$, black block, 0.520×0.320×0.100 mm, monoclinic space group $P2_1/c$, a = 10.28220(10) Å, b = 21.5158(2) Å, c = 17.1270(2) Å, α = 90°, β = 92.5340(10)°, γ = 90°, $V=3785.30(7)$ Å^3, T = 100.00(10) K, Z = 4, $\rho_{calcd.}=1.178$ g cm^{-3}, $\mu=0.979$ mm^{-1}, $F(000)=1440$, 40527 reflections in $h(-12/8)$, $k(-27/26)$, $l(-21/21)$ measured in the range $3.300°<\theta<77.575°$, 7951 independent reflections, 7951 observed reflections $[I>2\sigma(I)]$, 436 parameters, 0 restraints; all data: $R_1=0.0498$ and $wR_2=0.1248$, $I>2\sigma(I)$: $R_1=0.0455$ and $wR_2=0.1219$, *Goof* 1.070, largest difference peak/hole 0.700/−0.406 e Å^{-3}.

Crystal data for 1$^+$: $(C_{42}H_{48}N_4Ni)$ $(C_{24}H_{20}B)$, $M_r=986.76$, colorless block, 0.310×0.250×0.140 mm, monoclinic space group C2/c, a = 29.18590(10) Å, b = 11.86440(10) Å, c = 32.5491(2) Å, α = 90°, β = 100.9300(10)°, γ = 90°, $V=11066.42(13)$ Å^3, T = 100.00(10) K, Z = 8, $\rho_{calcd.}=1.185$ g cm^{-3}, $\mu=0.829$ mm^{-1}, $F(000)=4200$, 114119 reflections in $h(-31/36)$, $k(-15/14)$, $l(-41/41)$ measured in the range $2.765°<\theta<77.733°$, 11664 independent reflections, 11664 observed reflections $[I>2\sigma(I)]$, 661 parameters, 0 restraints; all data: $R_1=0.0403$ and $wR_2=0.0992$, $I>2\sigma(I)$: $R_1=0.0380$ and $wR_2=0.0975$, *Goof* 1.044, largest difference peak/hole 0.337/−0.428 e Å^{-3}.

Crystal data for 2$^+$: $(C_{42}H_{52}N_4Ni)$ $(C_{24}H_{20}B)$, $M_r=990.79$, colorless plate, 0.180×0.080×0.020 mm, monoclinic space group C2/c, a = 29.3145(6) Å, b = 11.9213(3) Å, c = 32.4240(7) Å, α = 90°, β = 101.200(2)°, γ = 90°, $V=11115.3(4)$ Å^3, T = 100.00(10) K, Z = 8, $\rho_{calcd.}=1.184$ g cm^{-3}, $\mu=0.826$ mm^{-1}, $F(000)=4232$, 51568 reflections in $h(-33/34)$, $k(-14/14)$, $l(-38/38)$ measured in the range $2.779°<\theta<67.079°$, 9836 independent reflections, 9836 observed reflections $[I>2\sigma(I)]$, 661 parameters, 0 restraints; all data: $R_1=$

0.1451 and $wR_2 = 0.3342$, $I > 2\sigma(I)$: $R_1 = 0.1223$ and $wR_2 = 0.3230$, *Goof* 1.130, largest difference peak/hole 0.810/−0.724 e Å^{-3}.

Crystal data for 3$^+$: $2(C_{54}H_{72}N_4Ni)$ $2(C_{24}H_{20}B) + 3(C_4H_8O)$, $M_r =$ 2526.45, colorless block, 0.321 × 0.191 × 0.099 mm, monoclinic space group $P2_1/n$, a = 13.77170(10) Å, b = 26.1741(2) Å, c = 20.9470(2) Å, $\alpha = 90°$, $\beta = 102.9370(10)°$, $\gamma = 90°$, $V = 7358.93(11)$ Å^3, T = 100.00(10) K, Z = 2, $\rho_{calcd.} = 1.140$ g cm^{-3}, $\mu = 0.738$ mm^{-1}, $F(000) = 2724$, 113809 reflections in $h(-17/17)$, $k(-30/32)$, $l(-26/26)$ measured in the range $2.745° < \theta < 74.504°$, 15036 independent reflections, 15036 observed reflections [$I > 2\sigma(I)$], 994 parameters, 444 restraints; all data: $R_1 = 0.0626$ and $wR_2 = 0.1537$, $I > 2\sigma(I)$: $R_1 = 0.0562$ and $wR_2 = 0.1482$, *Goof* 1.055, largest difference peak/hole 0.749/−0.412 e Å^{-3}.

Crystal data for 4$^+$: $(C_{54}H_{76}N_4Ni)$ $(C_{24}H_{20}B) + 2(C_4H_8O)$, $M_r = 1303.31$, colorless block, 0.420 × 0.210 × 0.040 mm, triclinic space group P-1, a = 13.4480(3) Å, b = 14.6097(3) Å, c = 19.4957(4) Å, $\alpha = 75.815(2)°$, $\beta = 85.411(2)°$, $\gamma = 81.820(2)°$, $V = 3671.71(14)$ Å^3, T = 100(2) K, Z = 2, $\rho_{calcd.} = 1.179$ g cm^{-3}, $\mu = 0.757$ mm^{-1}, $F(000) = 1410$, 69006 reflections in $h(-16/16)$, $k(-14/18)$, $l(-24/24)$ measured in the range $2.340° < \theta < 74.503°$, 14856 independent reflections, 14856 observed reflections [$I > 2\sigma(I)$], 909 parameters, 210 restraints; all data: $R_1 = 0.0609$ and $wR_2 = 0.1431$, $I > 2\sigma(I)$: $R_1 = 0.0526$ and $wR_2 = 0.1375$, *Goof* 1.027, largest difference peak/hole 0.655/−0.584 e Å^{-3}.

Crystal data for 5$^+$: $(C_{40}H_{62}N_2Ni)$ $(C_{24}H_{20}B)$, $M_r = 948.83$, yellow block, 0.460 × 0.400 × 0.140 mm, monoclinic space group C2/c, a = 16.92060(10) Å, b = 17.10430(10) Å, c = 18.8998(2) Å, $\alpha = 90°$, $\beta = 95.6240(10)°$, $\gamma = 90°$, $V = 5443.56(7)$ Å^3, T = 100.00(10) K, Z = 4, $\rho_{calcd.} = 1.158$ g cm^{-3}, $\mu = 0.805$ mm^{-1}, $F(000) = 2052$, 29083 reflections in $h(-20/21)$, $k(-21/17)$, $l(-23/23)$ measured in the range $3.683° < \theta < 74.499°$, 5546 independent reflections, 5546 observed reflections [$I > 2\sigma(I)$], 317 parameters, 0 restraints; all data: $R_1 = 0.0351$ and $wR_2 = 0.0884$, $I > 2\sigma(I)$: $R_1 = 0.0334$ and $wR_2 = 0.0872$, *Goof* 1.035, largest difference peak/hole 0.305/−0.399 e Å^{-3}.

Crystal data for 1^{+THF} and 1^{+BF4}: $2(C_{46}H_{56}N_4NiO)$, $C_{42}H_{48}N_4Ni$, $3(BF_4)$, $M_r = 2407.29$, yellow block, 0.300 × 0.080 × 0.040 mm, monoclinic space group I2/a, a = 15.74940(10) Å, b = 16.0733(2) Å, c = 51.0731(5) Å, $\alpha = 90°$, $\beta = 98.2310(10)°$, $\gamma = 90°$, $V = 12795.7(2)$ Å^3, T = 100.00(10) K, Z = 4, $\rho_{calcd.} = 1.250$ g cm^{-3}, $\mu = 1.101$ mm^{-1}, $F(000) = 5084$, 60448 reflections in $h(-18/18)$, $k(-19/18)$, $l(-61/61)$ measured in the range $2.885° < \theta < 67.080°$, 11415 independent reflections, 11415 observed reflections [$I > 2\sigma(I)$], 767 parameters, 0 restraints; all data: $R_1 = 0.0721$ and $wR_2 = 0.1565$, $I > 2\sigma(I)$: $R_1 = 0.0677$ and $wR_2 = 0.1547$, *Goof* 1.268, largest difference peak/hole 0.698/−0.395 e Å^{-3}.

Computational Details

Calculations were carried out using the TURBOMOLE V7.2 2017 program suite, a development of the University of Karlsruhe and the Forschungszentrum Karlsruhe GmbH, 1989–2007, TURBOMOLE GmbH, since 2007; available from http://www.turbomole.com.[35] Geometry optimizations were performed using (RI-)DFT calculations[36] on a m4 grid employing the PBE0[37] functional and a def2-SV(P)[38] basis set for all atoms with the exception of Ni, for which a def2-TZVP basis set was used. The structures of **1** and **1**$^+$ were fully optimized, vibrational frequencies were calculated at the same level of theory with the AOFORCE[39] module and all structures represented true minima without imaginary frequencies. For **1**$^+$, the unrestricted formulism was employed and a final $<S^2>$ value of 0.756 indicated an absence of any significant spin-contamination for a doublet spin state. More information on the calculations is provided in the Supporting Information.

2182812 (**2**), 2182813 (**2**$^+$), 2182814 (**1**$^{+THF}$), 2182815 (**5**$^+$), 2182816 (**1**$^+$), 2182817 (**4**$^+$), and 2182818 (**3**$^+$)

Deposition Numbers 2182812 (**2**), 2182813 (**2**$^+$), 2182814 (**1**$^{+THF}$), 2182815 (**5**$^+$), 2182816 (**1**$^+$), 2182817 (**4**$^+$), and 2182818 (**3**$^+$) contain the supplementary crystallographic data for this paper. These data are provided free of charge by the joint Cambridge Crystallographic Data Centre and Fachinformationszentrum Karlsruhe Access Structures service www.ccdc.cam.ac.uk/structures.

Acknowledgements

This work was supported by funds from the Julius-Maximilians-Universität Würzburg and the Deutsche Forschungsgemeinschaft (DFG RA720/12). Open Access funding enabled and organized by Projekt DEAL.

Conflict of Interest

The authors declare no conflict of interest.

Data Availability Statement

The data that support the findings of this study are available in the supplementary material of this article.

Keywords: Alkyl(amino)carbene · EPR spectroscopy · Metalloradicals · *N*-heterocyclic Carbene · Nickel ComplexCyclic

[1] a) P. P. Power, *Chem. Rev.* **2012**, *112*, 3482–3507; b) D. L. Kays, *Dalton Trans.* **2011**, *40*, 769–778; c) C. Y. Lin, P. P. Power, *Chem. Soc. Rev.* **2017**, *46*, 5347–5399.
[2] L. J. Taylor, D. L. Kays, *Dalton Trans.* **2019**, *48*, 12365–12381.
[3] a) J. M. Frost, K. L. M. Harriman, M. Murugesu, *Chem. Sci.* **2016**, *7*, 2470–2491; b) A. K. Bar, C. Pichon, J.-P. Sutter, *Coord. Chem. Rev.* **2016**, *308*, 346–380.
[4] P. P. Power, *J. Organomet. Chem.* **2004**, *689*, 3904–3919.
[5] a) T. Schaub, U. Radius, *Z. Anorg. Allg. Chem.* **2006**, *632*, 981–984; b) T. Schaub, M. Backes, U. Radius, *Chem. Commun.* **2007**, 2037–2039; c) T. Schaub, C. Döring, U. Radius, *Dalton Trans.* **2007**, 1993–2002; d) T. Schaub, U. Radius, *Z. Anorg. Allg. Chem.* **2007**, *633*, 2168–2172; e) T. Schaub, M. Backes, O. Plietzsch, U. Radius, *Dalton Trans.* **2009**, 7071–7079; f) T. Zell, T. Schaub, K. Radacki, U. Radius, *Dalton Trans.* **2011**, *40*, 1852–1854; g) B. Zarzycki, T. Zell, D. Schmidt, U. Radius, *Eur. J. Inorg. Chem.* **2013**, 2051–2058; h) J. H. J. Berthel, M. W. Kuntze-Fechner, U. Radius, *Eur. J. Inorg. Chem.* **2019**, 2618–2623; i) J. H. J. Berthel, L. Tendera, M. W. Kuntze-Fechner, L. Kuehn, U. Radius, *Eur. J. Inorg. Chem.* **2019**, 3061–3072; j) L. Tendera, T. Schaub, M. J. Krahfuss, M. W. Kuntze-Fechner, U. Radius, *Eur. J. Inorg. Chem.* **2020**, 3194–3207; k) L. Tendera, M. Helm, M. J. Krahfuss, M. W. Kuntze-Fechner, U. Radius, *Chem. Eur. J.* **2021**, *27*, 17849–17861; l) S. Sabater, D. Schmidt, H. Schmidt, M. Kuntze-Fechner, T. Zell, C. Isaac, N. Rajabi, H. Grieve, W. Blackaby, J. Lowe, S. Macgregor, M. Mahon, U. Radius, M. Whittlesey, *Chem. Eur. J.* **2021**, *27*, 13221–13224.
[6] a) T. Zell, M. Feierabend, B. Halfter, U. Radius, *J. Organomet. Chem.* **2011**, *696*, 1380–1387; b) T. Zell, U. Radius, *Z. Anorg. Allg. Chem.* **2011**, *637*, 1858–1862; c) T. Zell, P. Fischer, D. Schmidt, U. Radius, *Organometallics* **2012**, *31*, 5065–5073; d) D. Schmidt, T. Zell, T. Schaub, U. Radius, *Dalton Trans.* **2014**, *43*, 10816–10827; e) L. Kuehn, D. G. Jammal, K. Lubitz, T. B. Marder, U. Radius, *Chem. Eur. J.* **2019**, *25*, 9514–9521; f) M. W. Kuntze-Fechner, C. Kerpen, D. Schmidt, M. Häring, U. Radius, *Eur. J. Inorg. Chem.*

2019, 1767–1775; g) Y. M. Tian, X. N. Guo, I. Krummenacher, Z. Wu, J. Nitsch, H. Braunschweig, U. Radius, T. B. Marder, *J. Am. Chem. Soc.* **2020**, *142*, 18231–18242; h) Y.-M. Tian, X.-N. Guo, Z. Wu, A. Friedrich, S. A. Westcott, H. Braunschweig, U. Radius, T. B. Marder, *J. Am. Chem. Soc.* **2020**, *142*, 13136–13144.

[7] a) T. Schaub, U. Radius, *Chem. Eur. J.* **2005**, *11*, 5024–5030; b) T. Schaub, M. Backes, U. Radius, *J. Am. Chem. Soc.* **2006**, *128*, 15964–15965; c) T. Schaub, P. Fischer, A. Steffen, T. Braun, U. Radius, A. Mix, *J. Am. Chem. Soc.* **2008**, *130*, 9304–9317; d) T. Schaub, P. Fischer, T. Meins, U. Radius, *Eur. J. Inorg. Chem.* **2011**, 3122–3126; e) J. Zhou, J. H. Berthel, M. W. Kuntze-Fechner, A. Friedrich, T. B. Marder, U. Radius, *J. Org. Chem.* **2016**, *81*, 5789–5794.

[8] a) J. Zhou, M. W. Kuntze-Fechner, R. Bertermann, U. S. Paul, J. H. Berthel, A. Friedrich, Z. Du, T. B. Marder, U. Radius, *J. Am. Chem. Soc.* **2016**, *138*, 5250–5253; b) Y. Tian, X. Guo, M. Kuntze-Fechner, I. Krummenacher, H. Braunschweig, U. Radius, A. Steffen, T. B. Marder, *J. Am. Chem. Soc.* **2018**, *140*, 17612–17623.

[9] M. W. Kuntze-Fechner, H. Verplancke, L. Tendera, M. Diefenbach, I. Krummenacher, H. Braunschweig, T. B. Marder, M. C. Holthausen, U. Radius, *Chem. Sci.* **2020**, *11*, 11009–11023.

[10] See for example: a) C. A. Laskowski, G. L. Hillhouse, *J. Am. Chem. Soc.* **2008**, *130*, 13846–13847; b) S. Miyazaki, Y. Koga, T. Matsumoto, K. Matsubara, *Chem. Commun.* **2010**, *46*, 1932–1934; c) K. Zhang, M. Conda-Sheridan, S. R. Cooke, J. Louie, *Organometallics* **2011**, *30*, 2546–2552; d) D. D. Beattie, E. G. Bowes, M. W. Drover, J. A. Love, L. L. Schafer, *Angew. Chem.* **2016**, *128*, 13484–13489; *Angew. Chem. Int. Ed.* **2016**, *55*, 13290–13295; e) S. Pelties, E. Carter, A. Folli, M. F. Mahon, D. M. Murphy, M. K. Whittlesey, R. Wolf, *Inorg. Chem.* **2016**, *55*, 11006–11017; f) K. Matsubara, Y. Fukahori, T. Inatomi, S. Tazaki, Y. Yamada, Y. Koga, S. Kanegawa, T. Nakamura, *Organometallics* **2016**, *35*, 3281–3287; g) P. Zimmermann, C. Limberg, *J. Am. Chem. Soc.* **2017**, *139*, 4233–4242; h) I. Kalvet, Q. Guo, G. J. Tizzard, F. Schoenebeck, *ACS Catal.* **2017**, *7*, 2126–2132; i) R. J. Witzke, T. D. Tilley, *Organometallics* **2022**, *41*, 1565–1571.

[11] B. R. Dible, M. S. Sigman, A. M. Arif, *Inorg. Chem.* **2005**, *44*, 3774–3776.

[12] C. A. Laskowski, D. J. Bungum, S. M. Baldwin, S. A. Del Ciello, V. M. Iluc, G. L. Hillhouse, *J. Am. Chem. Soc.* **2013**, *135*, 18272–18275.

[13] M. I. Lipschutz, X. Yang, R. Chatterjee, T. D. Tilley, *J. Am. Chem. Soc.* **2013**, *135*, 15298–15301.

[14] C.-Y. Lin, J. C. Fettinger, F. Grandjean, G. J. Long, P. P. Power, *Inorg. Chem.* **2014**, *53*, 9400–9406.

[15] M. I. Lipschutz, T. D. Tilley, *Organometallics* **2014**, *33*, 5566–5570.

[16] R. C. Poulten, M. J. Page, A. G. Algarra, J. J. Le Roy, I. Lopez, E. Carter, A. Llobet, S. A. Macgregor, M. F. Mahon, D. M. Murphy, M. Murugesu, M. K. Whittlesey, *J. Am. Chem. Soc.* **2013**, *135*, 13640–13643.

[17] M. M. Schwab, D. Himmel, S. Kacprzak, V. Radtke, D. Kratzert, P. Weis, M. Wernet, A. Peter, Z. Yassine, D. Schmitz, E.-W. Scheidt, W. Scherer, S. Weber, W. Feuerstein, F. Breher, A. Higelin, I. Krossing, *Chem. Eur. J.* **2018**, *24*, 918–927.

[18] W. J. M. Blackaby, K. L. M. Harriman, S. M. Greer, A. Folli, S. Hill, V. Krewald, M. F. Mahon, D. M. Murphy, M. Murugesu, E. Richards, E. Suturina, M. K. Whittlesey, *Inorg. Chem.* **2022**, *61*, 1308–1315.

[19] A. J. Arduengo, S. F. Gamper, J. C. Calabrese, F. Davidson, *J. Am. Chem. Soc.* **1994**, *116*, 4391–4394.

[20] N. D. Harrold, A. R. Corcos, G. L. Hillhouse, *J. Organomet. Chem.* **2016**, *813*, 46–54.

[21] a) A. A. Danopoulos, D. Pugh, *Dalton Trans.* **2008**, 30–31; b) K. Matsubara, S. Miyazaki, Y. Koga, Y. Nibu, T. Hashimura, T. Matsumoto, *Organometallics* **2008**, *27*, 6020–6024.

[22] K. C. Mondal, P. P. Samuel, Y. Li, H. W. Roesky, S. Roy, L. Ackermann, N. S. Sidhu, G. M. Sheldrick, E. Carl, S. Demeshko, S. De, P. Parameswaran, L. Ungur, L. F. Chibotaru, D. M. Andrada, *Eur. J. Inorg. Chem.* **2014**, 818–823.

[23] a) U. Radius, F. M. Bickelhaupt, *Organometallics* **2008**, *27*, 3410–3414; b) U. Radius, F. M. Bickelhaupt, *Coord. Chem. Rev.* **2009**, *253*, 678–686.

[24] a) J. C. Green, B. J. Herbert, *Dalton Trans.* **2005**, 1214–1220; b) J. C. Green, R. G. Scurr, P. L. Arnold, F. Geoffrey, N. Cloke, *Chem. Commun.* **1997**, 1963–1964; c) M. C. MacInnis, J. C. DeMott, E. M. Zolnhofer, J. Zhou, K. Meyer, R. P. Hughes, O. V. Ozerov, *Chem.* **2016**, *1*, 902–920.

[25] Q. Lin, G. Dawson, T. Diao, *Synlett* **2021**, *32*, 1606–1620.

[26] a) U. S. D. Paul, M. J. Krahfuß, U. Radius, *Chem. Unserer Zeit* **2018**, *53*, 212–223; b) U. S. D. Paul, U. Radius, *Eur. J. Inorg. Chem.* **2017**, 3362–3375; c) U. S. D. Paul, U. Radius, *Organometallics* **2017**, *36*, 1398–1407.

[27] J. Attner, U. Radius, *Chem. Eur. J.* **2001**, *7*, 783–790.

[28] a) R. A. Schunn, S. D. Ittel, M. A. Cushing, R. Baker, R. J. Gilbert, D. P. Madden, *Inorg. Synth.* **1990**, *28*, 94–98; b) J. W. Wielandt, D. Ruckerbauer, T. Zell, U. Radius, *Inorg. Synth.* **2010**, *35*, 120–125.

[29] a) X. Bantreil, S. P. Nolan, *Nat. Protoc.* **2011**, *6*, 69–77; b) A. J. Arduengo, H. V. R. Dias, R. L. Harlow, M. Kline, *J. Am. Chem. Soc.* **1992**, *114*, 5530–5534; c) A. J. Arduengo, R. Krafczyk, R. Schmutzler, H. A. Craig, J. R. Goerlich, W. J. Marshall, M. Unverzagt, *Tetrahedron* **1999**, *55*, 14523–14534.

[30] a) V. Lavallo, Y. Canac, C. Präsang, B. Donnadieu, G. Bertrand, *Angew. Chem.* **2005**, *117*, 5851–5855; *Angew. Chem. Int. Ed.* **2005**, *44*, 5705–5709; b) R. Jazzar, R. D. Dewhurst, J.-B. Bourg, B. Donnadieu, Y. Canac, G. Bertrand, *Angew. Chem.* **2007**, *119*, 2957–2960; *Angew. Chem. Int. Ed.* **2007**, *46*, 2899–2902; c) P. Bissinger, H. Braunschweig, A. Damme, I. Krummenacher, A. K. Phukan, K. Radacki, S. Sugawara, *Angew. Chem.* **2014**, *126*, 7488–7491; *Angew. Chem. Int. Ed.* **2014**, *53*, 7360–7363.

[31] D. N. Hendrickson, Y. S. Sohn, H. B. Gray, *Inorg. Chem.* **1971**, *10*, 1559–1563.

[32] S. Stoll, A. Schweiger, *J. Magn. Reson.* **2006**, *178*, 42–55.

[33] K. Matsubara, K. Ueno, Y. Shibata, *Organometallics* **2006**, *25*, 3422–3427.

[34] G. Sheldrick, *Acta Crystallogr. Sect. A* **2015**, *71*, 3–8.

[35] a) F. Furche, R. Ahlrichs, C. Hättig, W. Klopper, M. Sierka, F. Weigend, *WIREs Comput. Mol. Sci.* **2014**, *4*, 91–100; b) R. Ahlrichs, M. Bär, M. Häser, H. Horn, C. Kölmel, *Chem. Phys. Lett.* **1989**, *162*, 165–169.

[36] a) M. Sierka, A. Hogekamp, R. Ahlrichs, *J. Chem. Phys.* **2003**, *118*, 9136–9148; b) O. Treutler, R. Ahlrichs, *J. Chem. Phys.* **1995**, *102*, 346–354; c) M. Häser, R. Ahlrichs, *J. Comput. Chem.* **1989**, *10*, 104–111.

[37] a) A. D. Becke, *Phys. Rev. A* **1988**, *38*, 3098–3100; b) J. P. Perdew, *Phys. Rev. B* **1986**, *33*, 8822–8824.

[38] a) F. Weigend, R. Ahlrichs, *Phys. Chem. Chem. Phys.* **2005**, *7*, 3297–3305; b) K. Eichkorn, F. Weigend, O. Treutler, R. Ahlrichs, *Theor. Chem. Acc.* **1997**, *97*, 119–124; c) K. Eichkorn, O. Treutler, H. Öhm, M. Häser, R. Ahlrichs, *Chem. Phys. Lett.* **1995**, *242*, 652–660; d) A. Schäfer, C. Huber, R. Ahlrichs, *J. Chem. Phys.* **1994**, *100*, 5829–5835.

[39] P. Deglmann, K. May, F. Furche, R. Ahlrichs, *Chem. Phys. Lett.* **2004**, *384*, 103–107.

Manuscript received: June 30, 2022
Revised manuscript received: July 26, 2022
Accepted manuscript online: August 4, 2022